Quantification of Casting Skin in Ductile and Compacted Graphite Irons and Its Effect on Tensile Properties

D.M. Stefanescu, S. Wills, J. Massone
The Ohio State University, Columbus Ohio

F. Duncan
Ashland Casting Solutions, Columbus Ohio

ABSTRACT

The mechanical properties of ductile (DI) and compacted graphite (CG) irons are measured and reported on standard machined specimens (as per ASTM). However, most castings retain most of the as-cast surface. This surface layer (the *casting skin*) includes both surface and subsurface features. Because of the casting skin, the mechanical properties of the part are typically significantly lower than those found on standard ASTM machined specimens.

The technical objectives of this research were to identify the individual features that together define skin quality in DI and CGI, to develop a method for the measurement of skin thickness, and to quantify the influence of the skin of thin wall (2 to 6 mm) DI castings on its tensile properties.

The features of the casting skin include surface (roughness) and subsurface (graphite degradation, graphite depletion, pearlitic rim) elements. Graphite shape measurements were used to evaluate graphite degradation. Graphite area measurements were used to determine the thickness of the graphite depleted layer. Microhardness measurements are useful when a pearlitic rim occurs. The average thickness of the skin for thin wall DI castings ranged from 0.15 to 0.45mm, while for CGI it ranged from 0.7 to 2.5mm.

It was found as expected that the strength decreased with thicker casting skin. The tensile and yield strength skin factor (ratio between the strength of as-cast and machined test plates) was about 0.93. This should be viewed as an upper limit, as only one of the surfaces of the mechanical properties test plate was as-cast. More significant reduction in strength should be expected.

Diffusion calculations confirmed that graphite degradation, graphite depletion and the pearlitic rim are the result of magnesium and carbon depletion at the mold/metal interface because of their oxidation. Alternatively, carbon diffusion from the mold can also result in pearlitic rim formation.

INTRODUCTION

The mechanical properties of DI, as those of most metallic materials, are measured on and reported (as per ASTM) on standard machined specimens. However, most castings retain most of the as-cast surface. This surface layer, commonly referred to as the *casting skin*, includes both surface and subsurface, and is typically incorporated in the term *surface quality*. Because of the casting skin, the mechanical properties of the part may be significantly different from those found on the standard ASTM specimens machined from the same casting. It is expected that as the thickness of the casting decreases, the relative effect of the skin on the mechanical properties increases. This issue has received only limited attention.[1,2,3,]

Recent research has demonstrated that light weight DI castings can be produced by reducing the wall thickness. Their static mechanical properties are fully compatible with ASTM requirements.[4] However, it was also found that, when the tests are performed on non machined samples and not on the standard fully machined specimens, and these properties depend heavily on surface quality. It is therefore important to further investigate the impact of casting skin on the mechanical properties and the machinability of light weight DI castings.

Industrial experience with compacted graphite iron (CGI) motor blocks shows that one of the main defects encountered in these castings is the occurrence of a graphite degradation layer (flake graphite skin). There are no clear solutions for this problem at this time.

The technical objectives of this research work included:

- identification of the individual features that together define skin quality (*e.g.*, surface roughness, subsurface microstructure, subsurface graphite morphology, microstructure gradient, and microhardness gradient)of DI and CGI;
- development of a method for characterization of skin quality;
- quantification of the influence of the skin of thin wall (2 to 6 mm) ductile iron (TWDI) castings on its tensile properties.

LITERATURE BACKGROUND

Goodrich and Lobenhofer[1] showed that there is a tendency towards decreasing the strength and elongation of DI because of the casting skin in the as-cast tensile test sample. They found a larger effect on the smaller castings, and reported different skin quality generated by different molding materials. DI samples cast in chemically bonded sand exhibited a surface layer of about 1.3 mm depth with degenerated graphite shapes and other microstructural anomalies. The matrix microstructure of the surface layer showed a pearlitic matrix, while the bulk of the sample exhibited ferritic-pearlitic matrix.

Dix *et al*. [4] demonstrated that the tensile strength of TWDI is 17% lower on sand-blast as-cast plates as compared with machined plates, and that slight grinding of the surface may result in 13% improvement (Fig. 1). Similar effects were documented by Labreque *et al*. [5]

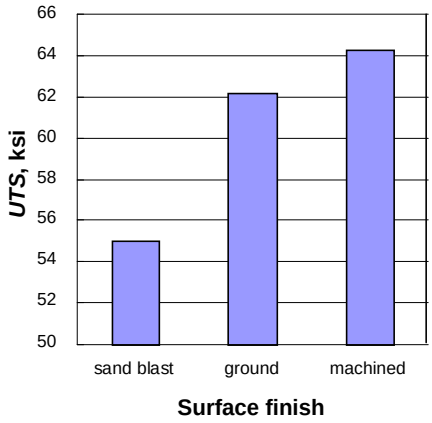

Fig. 1. Average tensile strength of TWDI as a function of surface finish. [4]

Mampaey *et al*. [2] studied the influence of the casting skin on gray iron. Fig. 2 shows the change in ultimate tensile strength (UTS) as the diameter of a 20mm sand cast round bar was gradually decreased to 8mm by machining. There is a marked increase in UTS as a layer of about 1 mm is removed from the sample. It was concluded that the cause of the decrease in strength in the presence of the casting skin was the formation of type D graphite at the surface layer, and, to a lesser extent, the increased ferrite content at the surface. Fig. 3 shows that there is a large amount of D graphite in the subsurface layer. The skin effect on strength was negligible for the lower strength gray irons, while it was of about 20% for a 300 MPa gray iron. Although specific for gray irons, Mampaey's study is useful to exemplify the relevance of the skin quality on iron castings.

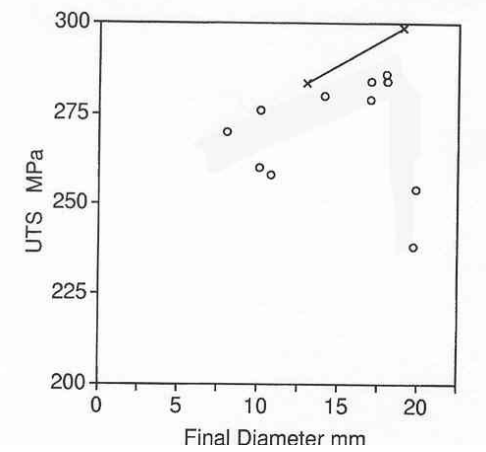

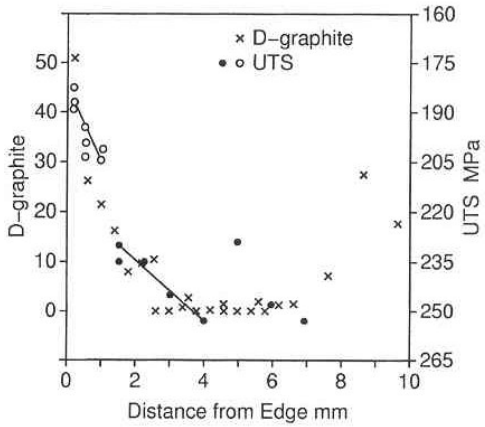

Fig. 2. The tensile strength of gray iron as a function of sample diameter. Different diameters are obtained by machining a 20mm sand cast round bar. [2]

Fig. 3. Amount of type-D graphite along the casting radius of a 20mm sand cast round gray iron bar. [2]

Aufderheide *et al*. [6] performed a systematic study on process variables (binder, coating, sand fineness, pouring temperature, and magnesium and inoculation level) that affect the casting skin of TWDI castings. They noted that sand fineness and magnesium level have the higher contributions to the skin effect.

Duncan and Kroker [7] analyzed lamellar graphite skin formation on the surface of CG iron. They concluded that slow cooling rates and small undercooling promote flake graphite growth, and that skin transition is caused by an imbalance between spheroidizing, primary and gaseous elements in the iron composition. The authors suggested that thermal gradient along the specimen height may be responsible for the wedge-shaped formation of skin in the vertical experimental samples.

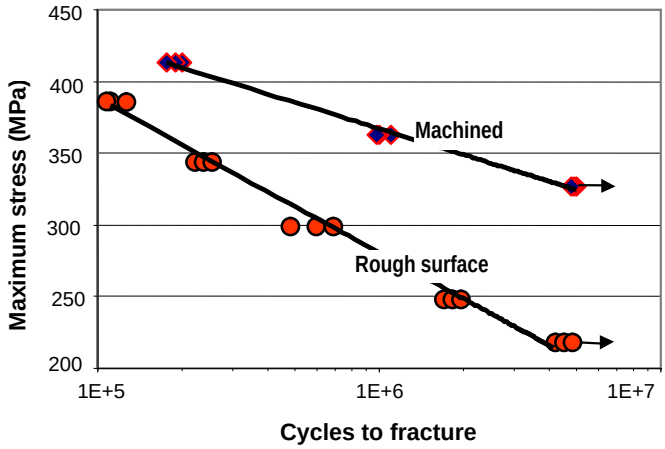

Fig. 4. Influence of surface finish on bending fatigue. [8]

Since surface finish seems to have such a significant effect on static mechanical properties, it is expected that the effect on fatigue properties will be even more remarkable. Unfortunately there is a paucity of data in the literature. As shown in Fig. 4, a "rough surface" can substantially decrease the fatigue limit.[8] However, the graph does not include any quantification of the surface quality. Labrecque *et al*. [9] concluded from experiments on TWDI (4 and 6 mm thickness) that the fatigue endurance limit (tensile stress) on machined samples is 2 to 19% higher as compared to the results obtained for samples having their as-cast surface exposed to the cyclic stresses.

Because findings of previous research[4] have suggested that there is a roughness threshold above which tensile strength decreases significantly (see Fig. 5), there is a clear need to identify a critical skin quality above which casting properties decrease dramatically.

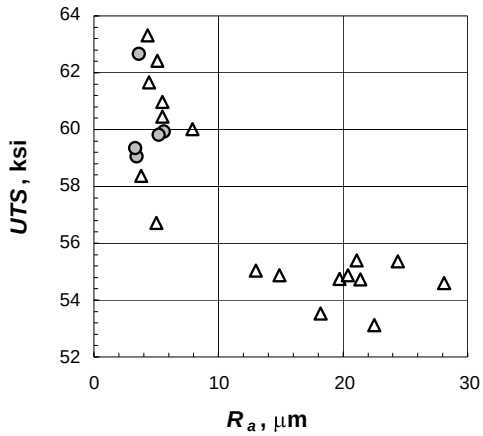

Fig. 5. The influence of surface roughness on tensile strength and elongation. [4]

SKIN QUALITY DEFINITION AND MEASUREMENT

A preliminary analysis of the factors that may account for the decreased static mechanical properties of TWDI measured on skin-covered specimens resulted in the identification of a number of responsible features:

- The surface roughness may be acting as stress concentrator.
- Surface cracks, other than roughness, may be present at the surface, nucleating fracture.
- Irregular graphite shapes present at the surface, such as compacted or exploded graphite, may account for a weaker skin.
- The matrix microstructure in the subsurface layer may be different than the bulk matrix of the casting (pearlite rim, graphite depletion).

To establish the methodology for skin quality measurement both DI test plates (poured at the Univ. of Alabama) and CGI test coupons (poured at Ashland Inc.) were used. The skin features of interest and the measurements performed in this work for the characterization of these features are presented in Table 1. As the roughness is a surface feature and is not related to the skin thickness (subsurface feature), it was not included in the analysis of these samples.

METHODOLOGY FOR SKIN QUALITY MEASUREMENT OF DUCTILE IRON CASTINGS

In a previous AFS sponsored research the influence of a number of process variables on the tensile properties and surface roughness of thin-wall ductile iron (TWDI) castings was investigated. The test casting (Fig. 6) was a 3-plates vertical casting with plates of thickness 6, 2.5 and 3.5 mm, poured in alkyd-urethane resin-bonded molds (see ref. 10 for details of melting and casting). Extensive statistical analysis was conducted to evaluate the experimental results on 32 test-plates. The complete results have been reported in an AFS paper[10].

Table 1. Skin Features and Methods for Their Measurement

Skin feature		Measurement
Surface	surface roughness	roughness average
Subsurface	graphite morphology	graphite shape factors
	graphite depletion	graphite area
		graphite count
	subsurface matrix microstructure	pearlite area
		microhardness

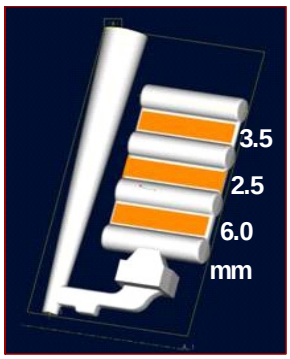

Fig. 6. Vertical plates casting with cylindrical risers.

For this research samples from heat 50602 (chemical composition 3.67%C, 2.92%Si, 0.04%Mg), mold no.8 (pouring temperature 1366°C) and mold 4 (pouring temperature 1400°C) were analyzed. The test-plates were cross sectioned and metallographic samples were prepared. On each metallographic sample a region of 1 mm depth from the sample surface was used in the analysis, as shown in Fig. 7.

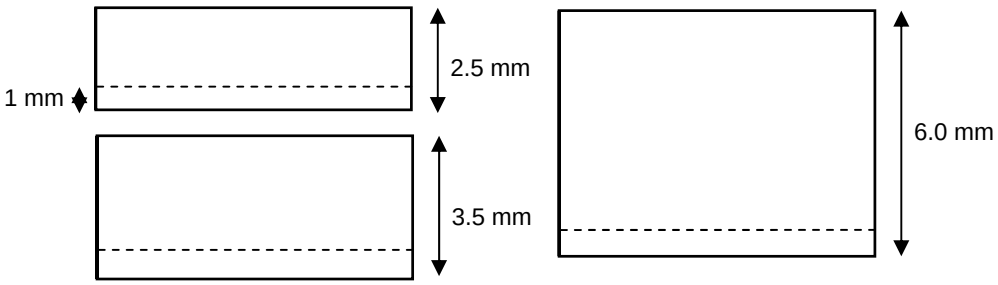

Fig. 7. Schematic of the 2.5, 3.5, and 6mm metallographic samples.

The microstructural features were evaluated using the Clemex Vision version 3.0 image analysis software and are summarized in Table 2. For additional details on these quantities the reader is referred to reference [11].

Table 2. Quantities Measured Through Image Analysis.

Quantity	Equation	Definitions
Sphericity	$S = 4 \cdot \pi \cdot Area / (Perimeter)^2$	
Roundness	$R = 4 \cdot Area / (\pi l_m^2)$	l_m : maximum axis length of the particle
	$R = 4 \cdot \pi \ Area / (r^2)$	r : radius of the circumscribed circle
Compactness	$C = 4 \cdot \pi \cdot Area / (Convex\ Perimeter)^2$	
Aspect ratio	$A_{ratio} = Length / Diameter\ circular$	
	$A_{ratio} = Length\ of\ longest\ feret / Length\ of\ shortest\ feret$	
Average area		
Fraction pearlite		measured after 4% Nital etching

An image analysis routine was created to conduct graphite shape and pearlite content measurements. In the routine, a 0.4×0.1mm frame at a magnification of 200X was created as a boundary for the measurements. The gray threshold was adjusted for the appropriate graphite or pearlite measurement. For the pearlite measurement, the threshold was adjusted to remove the graphite nodules from the measurement. Next in the routine, the total area and average area were measured, followed by the object measurements of sphericity, roundness, aspect ratio, and compactness.

This routine was performed on a number of consecutive frames sufficient to cover the depth of the casting skin. Data was collected for each of the ten frames then an average value for each frame was calculated. Microhardness measurements were taken on the 6mm sample from molds 6, 8, and 4 every 0.1mm. Measurements were made using a number of consecutive frames based on the depth of the casting skin. The routines are presented in Fig. 8.

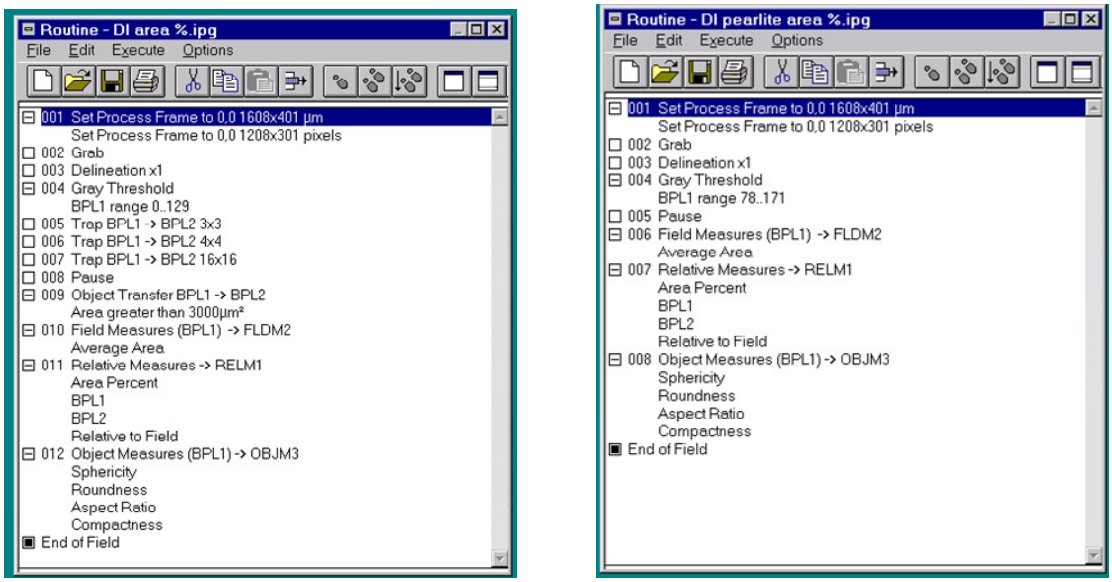

Fig. 8. Image analysis routines for measuring graphite shape (left) and percent pearlite (right).

The tabulated experimental results for mold 8 are presented in Table 3. Additional data on other molds can be found in ref. 12. The data in Table 3 were used to plot the variation of the average graphite shape parameters and the graphite area from the surface to the inside of the sample. An example of the analysis can be seen by examining Fig. 9. It is seen that all shape parameters increase rapidly until a certain subsurface depth (0.15-0.25mm), after which the numbers remain relatively constant (Fig. 9 left). The same is true for the graphite area (Fig. 9 right) where the values pick at 0.25mm. Clearly, the average area is a more reliable indicator of skin depth than graphite shape factors.

Table 3 Average Values for the Graphite Shape and Area, Mold 8.

Field	Distance (mm)	Sphericity	Round-ness	Compact-ness	Average shape factor	Avg. Area (μm^2)
2.5mm thick plates						
1	0.05	0.55	0.60	0.74	0.63	71.85
2	0.15	0.60	0.58	0.75	0.64	126.34
3	0.25	0.61	0.64	0.79	0.68	174.77
4	0.35	0.53	0.53	0.71	0.59	127.62
5	0.45	0.55	0.60	0.78	0.64	180.47
6	0.55	0.57	0.58	0.76	0.64	137.47
7	0.65	0.55	0.57	0.76	0.63	148.38
8	0.75	0.59	0.63	0.78	0.67	167.53
9	0.85	0.62	0.69	0.84	0.72	214.14
10	0.95	0.55	0.57	0.75	0.62	131.00
3.5mm thick plates						
1	0.05	0.51	0.51	0.70	0.57	42.54
2	0.15	0.56	0.59	0.76	0.64	144.59
3	0.25	0.53	0.58	0.74	0.62	189.67
4	0.35	0.61	0.63	0.79	0.68	152.96
5	0.45	0.63	0.62	0.79	0.68	180.44
6	0.55	0.66	0.60	0.78	0.68	141.50
7	0.65	0.59	0.64	0.79	0.67	142.00
8	0.75	0.57	0.60	0.78	0.65	189.85
9	0.85	0.59	0.62	0.79	0.67	176.52
10	0.95	0.58	0.60	0.78	0.65	131.61
6mm thick plates						
1	0.05	0.49	0.40	0.57	0.49	37.33
2	0.15	0.50	0.55	0.72	0.59	283.18
3	0.25	0.51	0.53	0.70	0.58	459.23
4	0.35	0.47	0.55	0.73	0.58	419.36
5	0.45	0.50	0.65	0.81	0.65	384.72
6	0.55	0.46	0.56	0.71	0.58	311.38
7	0.65	0.47	0.54	0.72	0.58	320.86
8	0.75	0.50	0.55	0.73	0.59	364.59
9	0.85	0.49	0.64	0.79	0.64	459.04
10	0.95	0.43	0.45	0.65	0.51	360.49

Fig. 10 is a representative image of the unetched as-cast surface of a 3.5mm sample. These data imply that the thickness of the casting skin in these samples is about 0.15 to 0.25mm, and is not significantly influenced by the thickness of the plate.

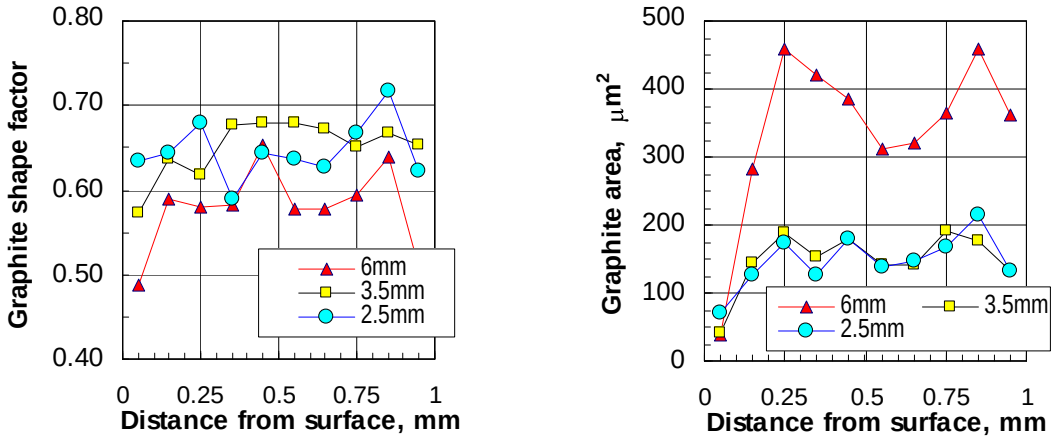

Fig. 9. Graphite shape (left) and graphite area (left) variation from the surface inward for plates from mold 8.

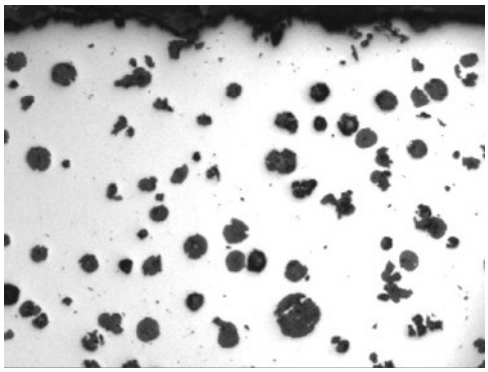

Fig. 10. Unetched microstructure next to the casting surface for a 3.5mm sample, mold 8. Note graphite depletion in the skin. Magnification 200X.

The percent pearlite for the 6mm sample was measured versus the distance from the as-cast surface (Fig. 11). There is a significant decrease in the amount of pearlite from the as-cast surface to 0.25mm into the sample. The Vickers microhardness measurements versus the distance from the as-cast surface are superimposed on the same graph. The hardness decreases with distance into the sample, confirming the decrease in the fraction pearlite from the surface inward. Fig. 12 is a representative image of the pearlite found near the as-cast surface on the 6mm sample and the microhardness imprints.

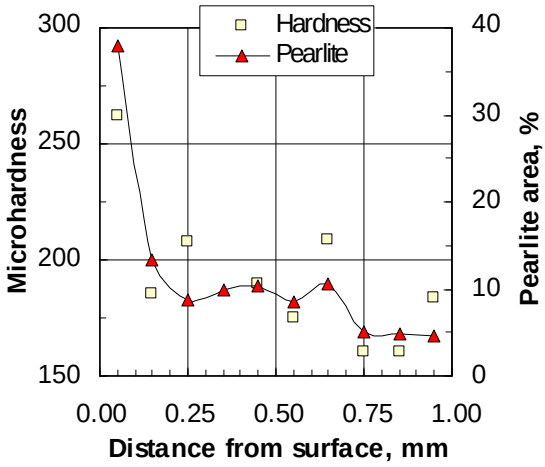

Fig. 11. Microhardness and pearlite area of the 6mm plate from mold 8.

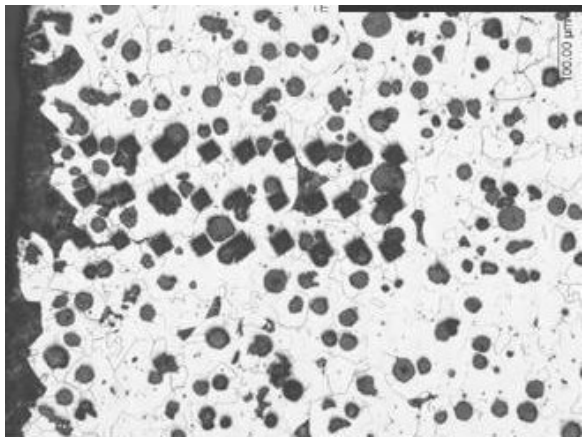

Fig. 12. Pearlite near the as-cast surface of the 6mm plate from mold 8 and microhardness imprints.

Flake graphite in the skin was only present on mold 4 heat 50602 (other details in ref. 10). Fig. 13 shows the Vickers microhardness measurements versus the distance from the as-cast surface. The hardness decreases with distance from the surface. Fig. 14 shows the flake graphite found near the as-cast surface. Only the 2.5 and 6mm samples of mold 4 contained flake graphite.

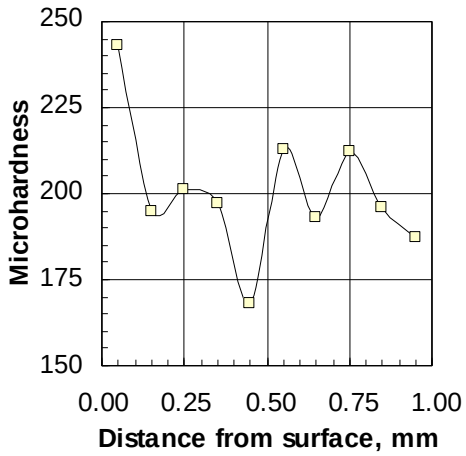

Fig. 13. Microhardness measurements on the 6mm plate from mold 4.

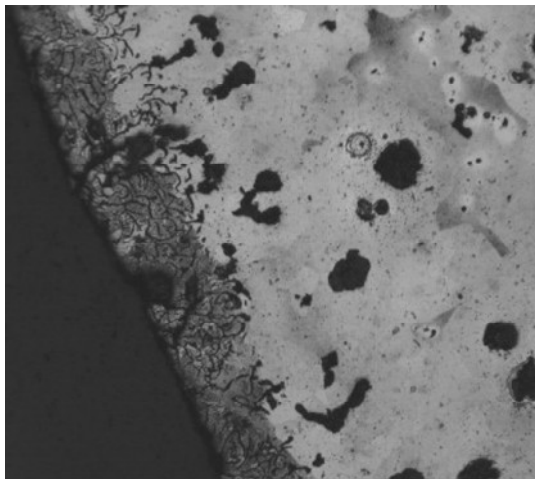

Fig. 14. Flake graphite at the as-cast surface of a plate in mold 4. Magnification 500X.

Based on these data it was concluded that the graphite shape parameters (sphericity, compactness and roundness) combined with graphite area measurements provide reliable information for the evaluation of graphite degradation in the casting skin. Microhardness measurements are useful when a pearlitic rim occurs. Based on graphite shape degradation, graphite depletion and microhardness measurements, the average thickness of the casting skin for the thin DI plates investigated ranges from 0.15 to 0.25mm.

METHODOLOGY FOR SKIN QUALITY MEASUREMENT OF COMPACTED GRAPHITE IRON CASTINGS

L-shaped sections of cylindrical test CG iron castings (Fig. 15) were received from Ashland Casting Solutions[7] for metallographic evaluation and microhardness measurements along the skin surface. Fig. 16 shows a schematic of the mold and a test casting assembly. It is a bottom gated three-part mold of an 8” cylinder diameter, which accommodates four 2”x2” cylindrical cores, and features a center located 8” riser. The molds were made with silica sand, GFN 55-60 and a phenolic urethane no-bake binder. The cores were made with zircon sand, GFN 108-112 and an cold-box binder at typical addition levels. While three samples were analyzed only results for one sample will be presented here, as the others were similar. Microstructural and microhardness investigation was conducted from the sample surface inward at four positions marked 0”, 0.5”, 1”, and 1.5”.

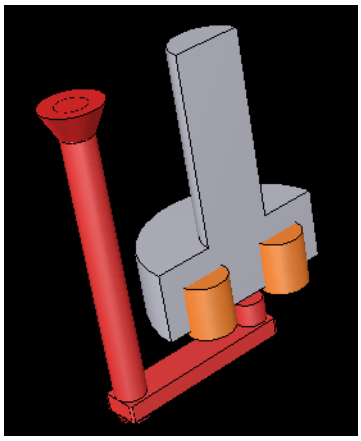

Fig. 15. Sectioned casting, cores and gating system (Ashland design)

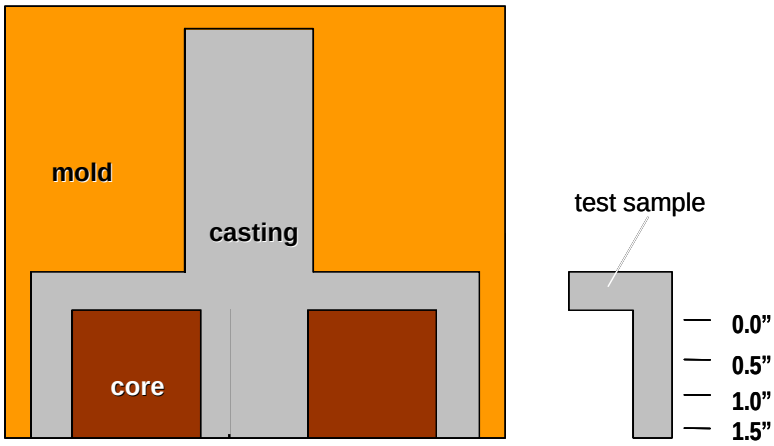

Fig. 16. Schematic of the mold and test sample. The numbers on the right are the metallostatic height.

Quantitative analysis was conducted as previously described. The routine was performed on several consecutive frames beginning at the as-cast surface. Data was collected for each frame and then an average value for each frame was calculated. For shape measurements at positions 0” and 0.5”, the routine was performed on 10 consecutive frames. For positions 1” and 1.5”, the measurements were made on 15 and 25 consecutive frames, respectively.

Microhardness measurements were performed every 0.1mm from the surface of the sample. For each position three imprints were measured. The recorded data is the average of these three measurements.

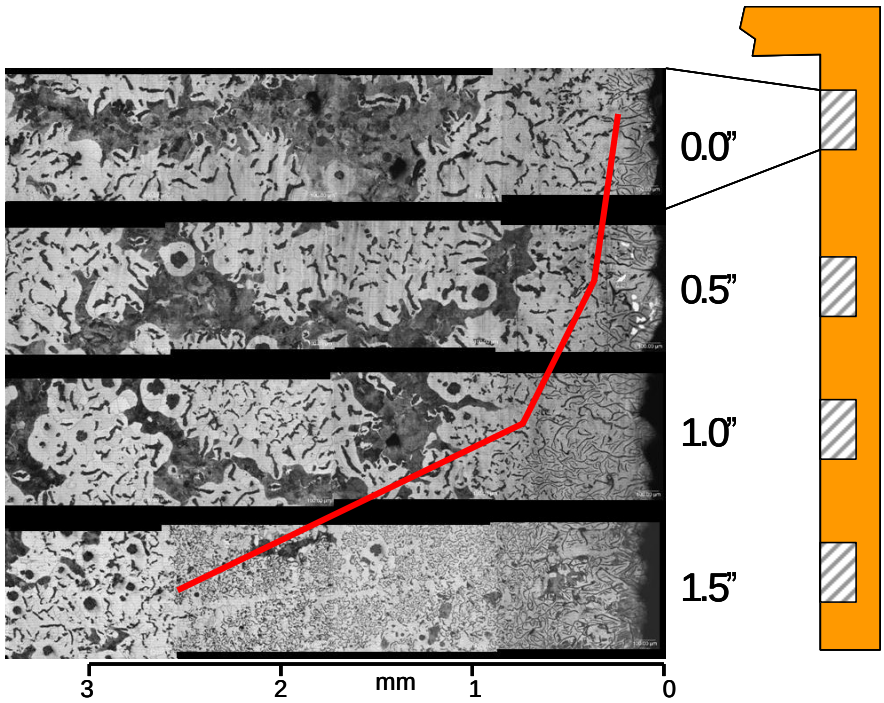

Fig. 17. Microstructure of casting skin in the CGI test casting in Fig. 15 as a function of relative metallostatic height.

Fig. 17 shows a montage at each position of the etched as-cast surface of the CG iron sample taken at 100X magnification. The following characteristic microstructural regions can be identified: flake graphite near the surface; next, fine flake and compacted to coarse compacted; coarse compacted and some spheroidal and exploded graphite further away from the surface. Position 1.5” has the largest amount of flake graphite while position 0” has the smallest amount. The amount of pearlite varies between positions. Position 1.5” has the smallest amount of pearlite while position 0” has the largest amount.

The measured data were used to plot the variation of the graphite shape parameters from the surface to the inside of the sample, for the 0”, 0.5”, 1”, and 1.5” positions. The graphs for the 0” and 1.5” positions are presented in Fig. 18, left column. The aspect ratio data are plotted in Fig. 18, right column.

From the plots in Fig. 18 it is possible to attempt to evaluate the thickness of the skin. All shape factors increase in value as the distance from the surface increases, reach a maximum and then stabilize more or less, although some significant variation may occur after the first maximum. The aspect ratio evolves in an opposite manner.

Fig. 19 shows the Vickers microhardness measurements versus the distance from the as-cast surface. Significant increase in hardness is seen at depths of 0.85mm and 1.25mm for positions 0.5” and 1”, respectively. This increase corresponds to the regions of pearlite found at these positions. For position 0” the pearlite hardness is only reached at a depth of 1.55mm.

The experimental data that correlate the thickness of the casting skin with the position (height) in the casting are summarized in Fig. 20. The thickness of the casting skin ranges from 0.7 to 2.5mm for the CGI investigated.

From the work on CGI presented here it is apparent that while microhardness may give an indication on the extent of the casting skin, it is not very reliable because of the discontinuities in the pearlite field and the influence of the graphite. It is still a useful indication when used in conjunction with the image analysis of graphite shape. The use of the average of the three parameters may also be interesting. Aspect ratio also gives useful information for CGI, while it does not seem to work for DI.

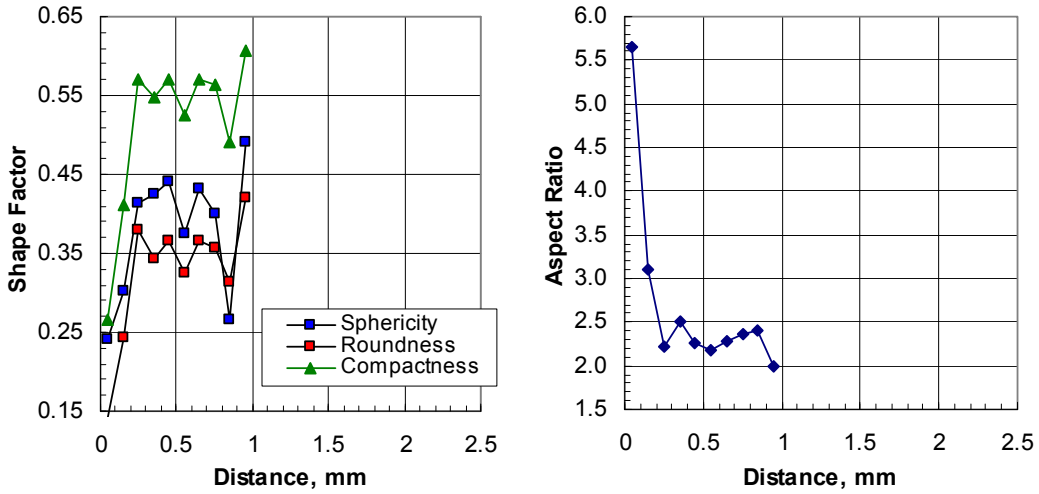

a) Position 0”

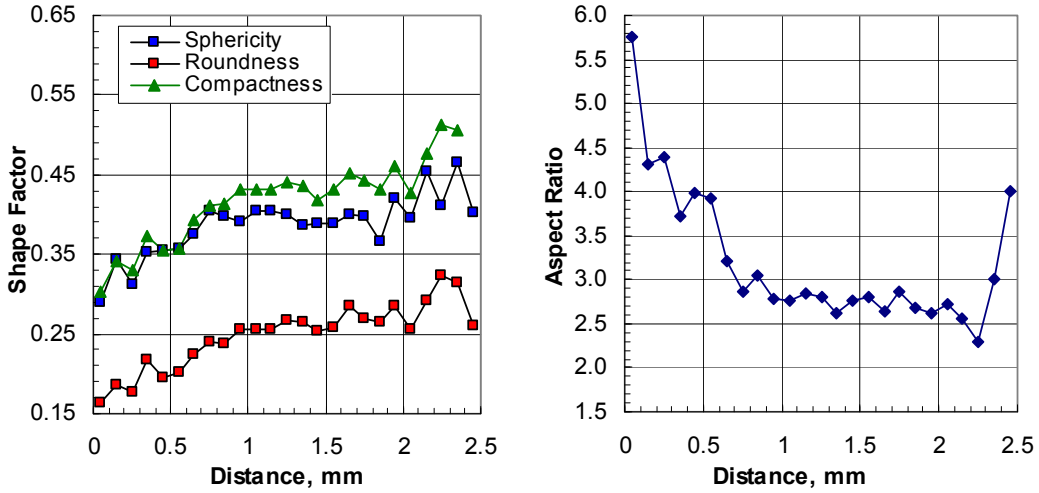

b) Position 1.5”

Fig. 18. Graphite shape variation with distance from surface for the 0” and 1.5” positions on the CGI sample.

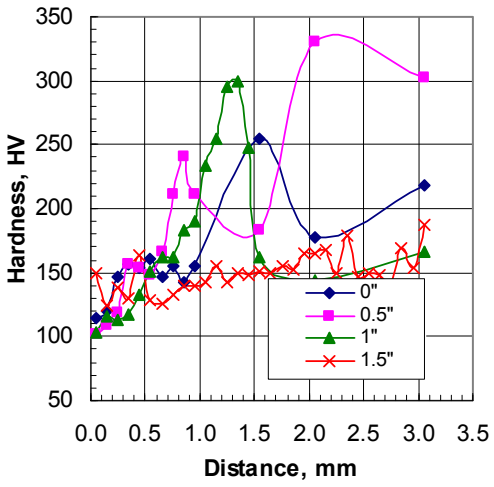

Fig. 19 Microhardness measurements at each position on the CG iron sample.

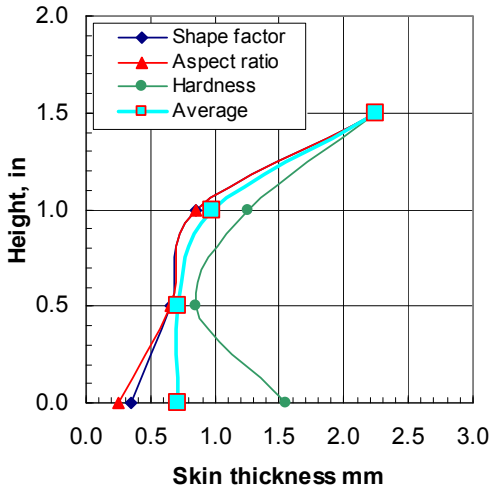

Fig. 20. The influence of the position in the casting (metallostatic height) on the thickness of the casting skin evaluated through three different parameters.

SKIN QUALITY QUANTIFICATION

EXPERIMENTAL APPROACH

While the methodology for skin quality measurement was developed for both DI and CGI, the quantification of the skin effect on mechanical properties involved only thin wall DI castings. A test casting was designed using the cad software Ironcad and the simulation software Magmasoft. The design objectives included: test casting large enough so that samples for tensile testing can be machined; mechanical testing to be performed on as-cast and machined samples; the characteristic cooling rate of the test sample should be about 10K/s; quiescent filling of the mold.

After a large number of computer experiments[12], the pattern shown in Fig. 21 was adopted. The pattern consisted of three plates of length 100mm, width 27mm, and thickness of 2.5, 4.0 and 6.0mm, respectively and an added filter.

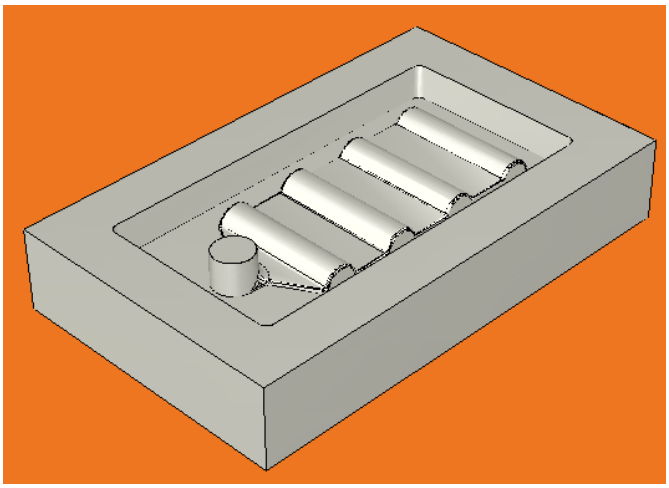

Fig. 21. Pattern used for mold production.

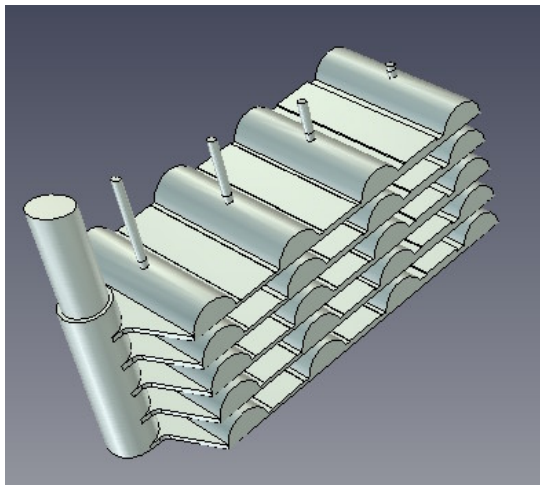

Fig. 22. Stacked and tilted casting.

Three stacked molds (one sodium silicate sand and two resin bonded sand) including five horizontal test castings (plates) each were produced (Fig. 22). The three molds were tilted 15 degrees for pouring. A 10 ppi filter was used in each mold. In addition to these molds buttons for metallographic analysis as well as chilled disks for chemical analysis were produced.

Table 4. Charge Composition and Chemical Analysis of Materials Used.

Material	Chemical composition, %						Addition, %
	C	Si	Mn	P	S	Mg	
Sorel pig iron	4.25	0.05	0.028	0.044	0.016	-	55
Steel scrap	0.2	0.5	0.2	0.03	0.02	-	5
CGI returns	3.47	2.23	0.15	0.033	0.016	-	40
FeSi50Mg5	NA	50	NA	NA	NA	5	1.73
FeSi75	NA	75	NA	NA	NA	NA	1.0

A 100lb melt was produced in the 300lb induction furnace at Ashland Inc. The charge composition is listed in Table 4. After melt down and correction the molten metal was transferred into a ladle and modified in stream with 1.73% FeSi50Mg5 alloy. After the completion of the Mg reaction, the slag was removed and 0.075% FeSi75 was added on top of the metal and then mixed as post inoculant. The molds and the buttons were poured at a temperature of 1350^{o}C. The castings were sand blasted.

EXPERIMENTAL RESULTS

Spectral chemical analysis was performed on chilled coins by Liberty Casting. The chemical analyses of the base metal and of the metal after Mg treatment and post-inoculation are given in Table 5.

Many attempts were made at measuring the surface roughness of the bottom side of the samples but, because the surface was obtained by scraping the corebox, the roughness was larger than the measurable limits of the instrument. To control the surface roughness variable the bottom side of all samples was machined to a smooth finish using a water-jet process.

Table 5. Chemical Analysis

Material	Chemical composition, %					
	C	Si	Mn	P	S	Mg
Base heat	3.76	1.80	0.080	0.054	0.012	-
treated ductile iron	NA	2.73	0.082	0.061	0.039	0.039

From each plate, two flat ASTM test samples for mechanical testing were machined as shown in Fig. 23. The dimensions of the test samples are given in Fig. 24.

The thickness of the casting skin was evaluated on the basis of graphite shape change as previously described. The complete tabulated measured data can be found in ref. 12.

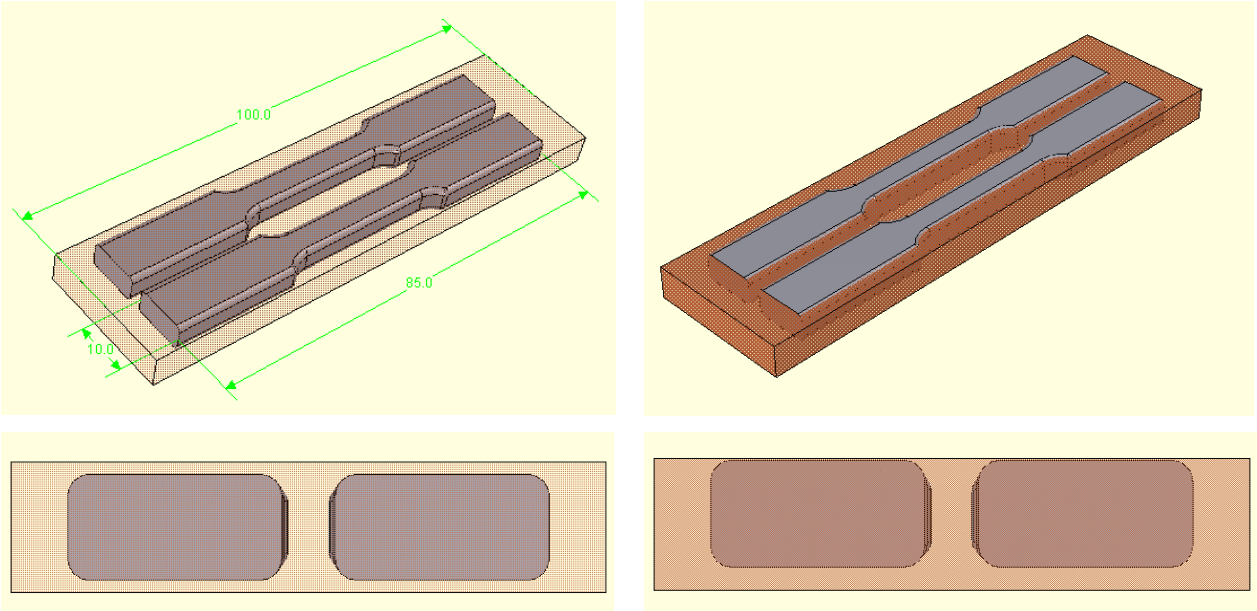

fully machined (M) ***machined only on bottom side (AC on top side)***

Fig. 23. Fully machined and partially machined (top surface as cast) samples.

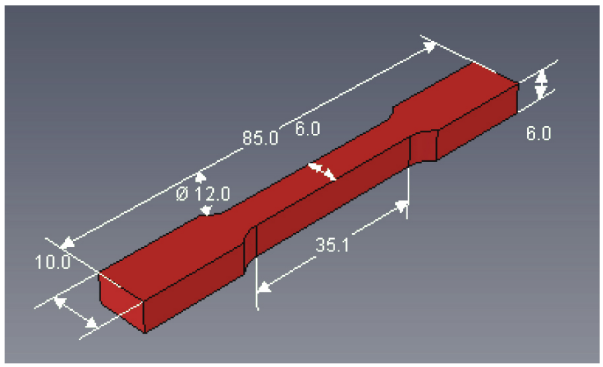

Fig. 24. Machined ASTM test sample.

Some examples of casting skin microstructure are presented in Figs. 25 and 26. Note the graphite depletion on the skin of the samples (Fig. 25) and the pearlitic rim on the etched samples (Fig. 26).

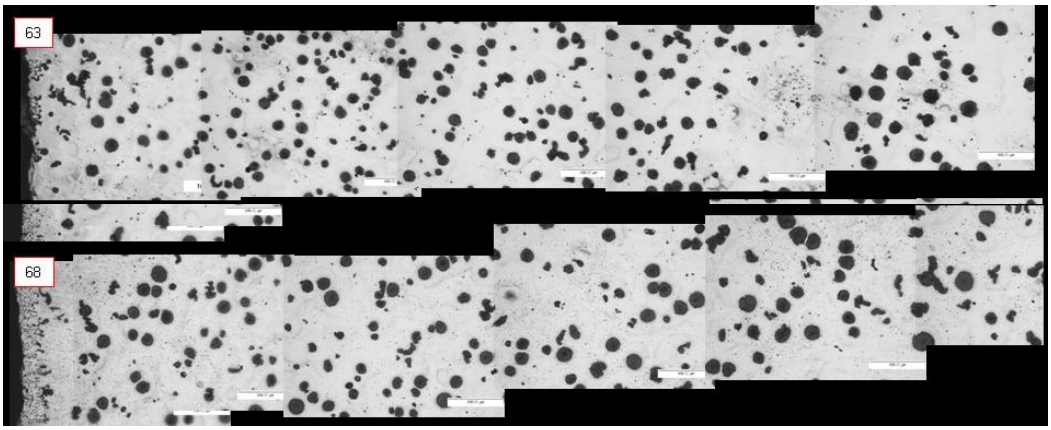

Fig. 25. Graphite morphology for samples #1ACp1/6mm (63) and p2/6mm (68) - unetched.

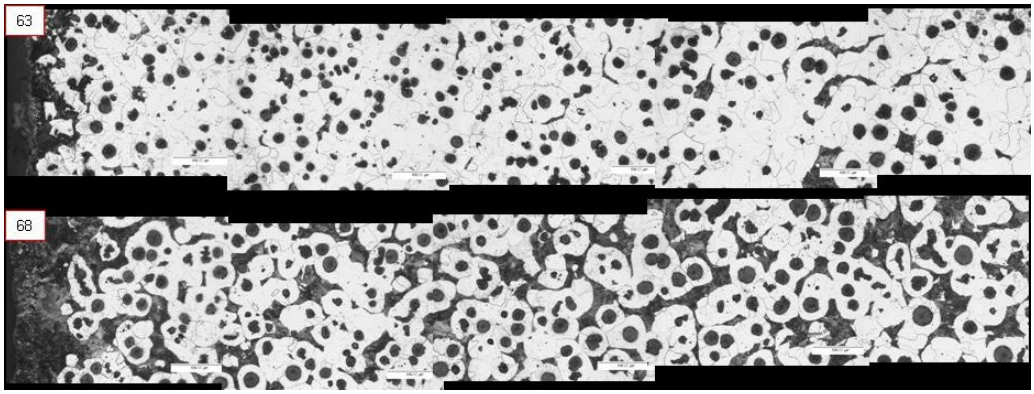

Fig. 26. Microstructure of samples #1ACp1/6mm (63) and p2/6mm (68) - etched.

The experimental measurements data are presented in Table 6. The pouring order is indicated by the # listed in front of the molding aggregate. The surface of the test samples was either as cast -AC (only the upper surface), or machined -M. The metallostatic height varies for each plat (test casting) because the molds were poured tilted 15 deg. with respect to the horizontal. It also increases from plate 1 to plate 4 because of the mold stacking. The roughness was measured only on the top surface. The bottom surface was too rough, as the mold surface was created by shaving the excess sand on top of the core box. The roughness was measured by the method described in reference 3 and reported as roughness average, R_a. All results for skin depth, roughness and mechanical properties are the average of two measurements.

DISCUSSION

VARIABLES AFFECTING THE CASTING SKIN

Correlation analysis was conducted on the as-cast samples for which the skin thickness was measured. The results are given in Table 7. It is seen that the casting skin increases in thickness as the plates become thinner (the correlation coefficient is -0.24). However, there is considerable scatter of data (Fig. 27). To explain this behavior an understanding of the mechanism of skin formation is required. This will be discussed in a later section.

The roughness increased with the metallostatic height (0.35). The correlation coefficient increased to 0.4 when all measured castings were included in the analysis (Fig. 28). This trend is reasonable, as mechanical penetration increases with metallostatic height.

Table 6. Experimental Measurements.

Mold	Surface	Plate	Thickness (mm)	Metallostatic height, mm	Skin depth (mm)	Roughness (Top) (μm)	UTS (ksi)	Yield Str. (ksi)	Elong. at fract. (%)
#1 sodium silicate	M	p1	4	33.4		11.27	64.5	41.6	13.8
	AC		6	66.9	0.25	15.93	53.9	37.2	7.3
	M	p2	4	59.7		21.56	65.4	42.8	10.0
	AC		6	93.2	0.15	15.80	71.5	57.4	5.2
	M	p3	2.5	71.5		15.33	63.9	45.5	11.0
	M		4	86.0		20.82	79.1	49.3	11.3
	M		6	119.5		25.14	78.8	48.4	10.9
	M	p4	2.5	97.8		22.39	66.1	44.2	21.7
	M		4	112.3		21.39	68.5	43.9	14.9
	M		6	145.8		22.55	67.8	43.6	17.4
#2 resin bonded	AC	p1	2.5	18.9	0.25	15.86	62.5	41.5	18.1
	AC		4	33.4	0.20	17.60	63.9	38.9	13.1
	AC		6	66.9	0.15	16.37	68.5	51.3	15.7
	AC	p2	2.5	45.2	0.23	19.91	60.8	39.2	13.2
	AC		4	59.7	0.35	22.69	62.4	39.0	18.2
	AC		6	93.2	0.27	26.27	62.2	40.8	16.7
	AC	p3	2.5	71.5	0.45	14.32	60.9	39.5	11.7
	AC		4	86.0	0.38	15.37	62.3	40.1	18.1
	AC		6	119.5	0.25	14.02	62.1	40.8	17.5
	AC	p4	2.5	97.8	0.28	18.02	63.9	42.0	17.0
	AC		4	112.3	0.35	19.84	63.1	42.8	16.4
	AC		6	145.8	0.35	22.18	67.3	43.4	18.9
	AC	p5	2.5	124.1	0.25	18.67	62.7	38.9	15.3
	AC		4	138.5	0.26	19.45	62.6	40.7	18.5
	AC		6	172.1	0.35	23.43	67.0	43.3	17.4
#3 resin bonded	M	p1	2.5	18.9	NM	21.28	69.9	45.8	10.8
	M		4	33.4	NM	19.68	62.8	36.4	17.1
	M		6	66.9	NM	24.40	63.7	42.5	20.2
	M	p2	2.5	45.2	NM	25.93	65.0	43.9	15.3
	M		4	59.7	NM	18.75	67.7	45.6	10.4
	M		6	93.2	NM	19.32	77.3	47.5	11.2
	M	p3	2.5	71.5	NM	23.46	63.0	41.6	14.9
	M		4	86.0	NM	19.26	65.9	45.0	14.0
	M		6	119.5	NM	22.11	75.4	49.2	7.1
	M	p4	2.5	97.8	NM	17.62	62.1	41.9	10.2
	M		4	112.3	NM	19.28	67.4	45.2	13.3
	M		6	145.8	NM	21.15	76.3	50.9	13.1
	M	p5	2.5	124.1	NM	25.41	62.6	44.2	14.5
	M		4	138.5	NM	23.60	63.7	43.2	17.0
	M		6	172.1	NM	29.38	66.1	44.5	15.7

Table 7. Correlation Analysis for All As-Cast Samples

As cast	*Skin depth*	*Roughness*
Plate thickness	-0.24	0.20
Metall. Height	0.28	0.35

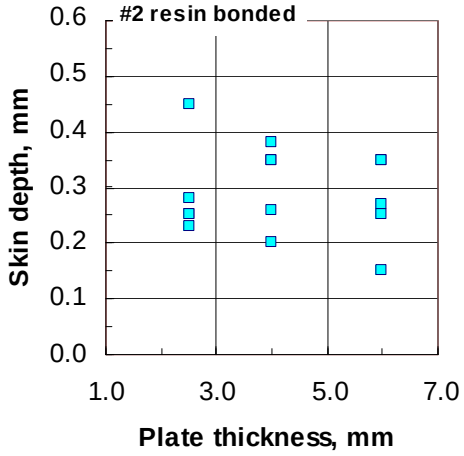

Fig. 27. Variation of the thickness of the skin depth with the thickness of the test plates.

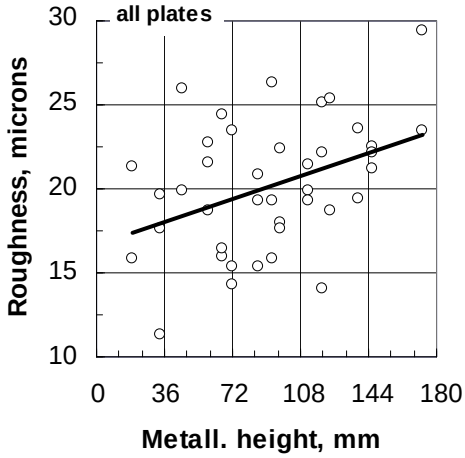

Fig. 28. Variation of measured roughness on the top surface of the plates with the metallostatic height.

VARIABLES AFFECTING THE TENSILE PROPERTIES

Correlation analysis was conducted only on the as-cast samples from mold #2, because the mechanical properties test samples had only one as-cast surface, while the samples from mold #1 had two as-cast surfaces. The results presented in Table 8 indicate that the tensile properties are favorably affected by increased plate thickness (Fig. 29) and metallostatic height, but negatively affected by thicker casting skin (Fig. 30). The increase of tensile properties with plate thickness is explained by the thinner skin associated with the thicker plates.

The effect of roughness is inconclusive. This is not surprising. Indeed, as shown in Fig. 5, a significant increase in strength occurs only at roughness below 10μm. For the analyzed samples the average roughness was considerably higher - 18.6μm.

Table 8. Correlation Analysis for As-Cast Samples (Mold #2)

As cast	*UTS*	*Yield Str.*	*Elong.*	*Skin depth*	*Roughness*	*Thickness*
Yield Strength	0.80	1.00				
Elongation	0.29	0.19	1.00			
Skin depth	-0.23	-0.33	0.07	1.00		
Roughness	0.21	-0.03	0.28	0.07	1.00	
Thickness	0.61	0.52	0.40	-0.11	0.37	1.00
Metall. Height	0.37	0.15	0.43	0.30	0.35	0.47

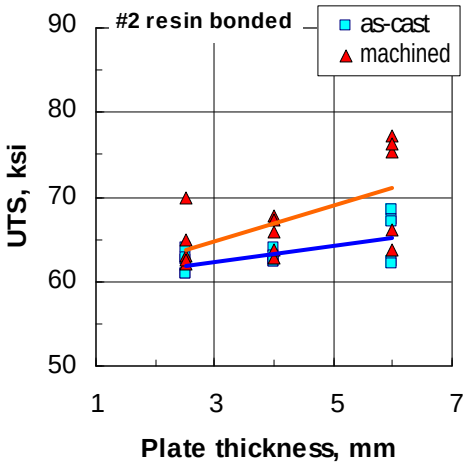

Fig. 29. Variation of tensile strength with the plate thickness.

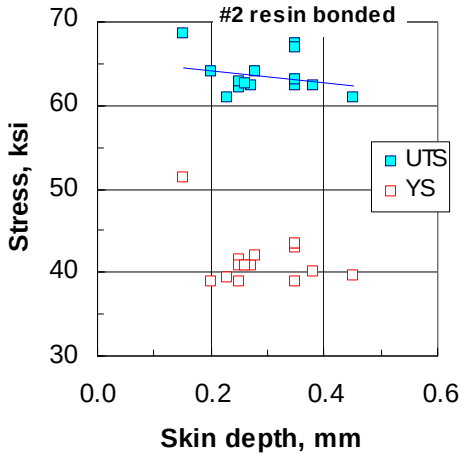

Fig. 30. Variation of tensile stress with the skin depth.

Results of correlation analysis on the machined samples are presented in Table 9. The trend of an increasing strength with plate thickness (Fig. 29) and metallostatic height is confirmed. The positive correlation between strength and metallostatic height may be the results of either i) higher material compactness with higher metallostatic pressure, or ii) higher plate thickness with higher metallostatic pressure resulting from the experimental setup (the plates within a casting follow the sequence 2.5, 4 and 6mm, with the 6mm being always higher than the other because of the tilting of the mold during pouring). Note that, unfortunately, for both as cast and machined samples metallostatic height correlates well with plate thickness (≥ 0.5).

Table 9. Correlation Analysis for Machined Samples

Machined	*UTS*	*Yield Str.*	*Elong.*	*Thickness*
Yield Str.	0.83	1.00		
Elongation	-0.46	-0.49	1.00	
Thickness	0.55	0.38	-0.04	1.00
Metall. Height	0.25	0.40	0.11	0.49

As expected the elongation decreases as strength increases (-0.46 for UTS and -0.49 for YS). This effect is less clear for as-cast samples (Fig. 31).

CALCULATION OF SKIN QUALITY

A skin quality factor for tensile strength is defined as the ratio between the as-cast (TS_{ac}) and machined (TS_m) tensile strength:

$$SF_{TS} = TS_{ac}/TS_m \qquad \text{Equation 1}$$

From the data in Table 6, the average values in Table 10 are obtained.

Table 10. Average Mechanical Properties on As-Cast and Machined Samples

Quantity	As-cast		Machined	
	Average	Range	Average	Range
UTS (ksi)	63.5	60.8-68.5	67.9	62.1-79.1
YS (ksi)	41.5	37.2-43.3	44.6	36.4-50.9

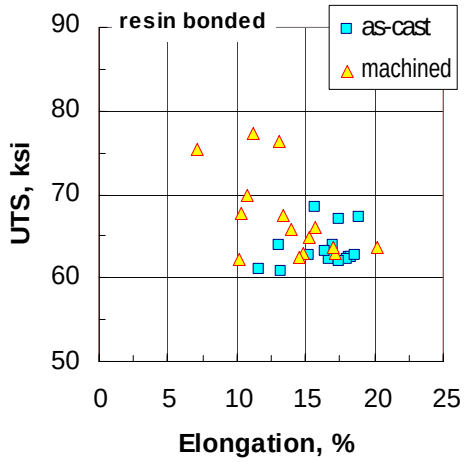

Fig. 31. Correlation between tensile strength and elongation.

Using Eq. 2 the average TS skin factor for these data is calculated as: $SF_{TS} = TS_{ac}/TS_m = 63.5/67.9 = 0.93$. Note that the same value is obtained for the yield strength skin factor.

To predict the skin factor, further quantification/calculation of skin quality must be performed using elements of characterization as shown in Fig. 32. They include: average roughness, R_a; skin thickness, t_{skin}; property gradient – describes the change of a certain quantity (e.g., nodularity, % pearlite, microhardness) over the thickness of the skin. The tensile specimens machined from plates of different thickness are tested in as cast condition. Linear regression analysis is then conducted to correlate *TS* to the various skin features. An equation having the following shape is produced:

$$TS_{ac} = a + b \cdot R_a + c \cdot t_{skin} + d \cdot dN/dx + \ldots \quad \text{Equation 2}$$

where a, b, c, d are coefficients to be determined from the regression analysis of the experiments, *dN/dx* is the nodularity gradient and others are as defined in Fig. 32.

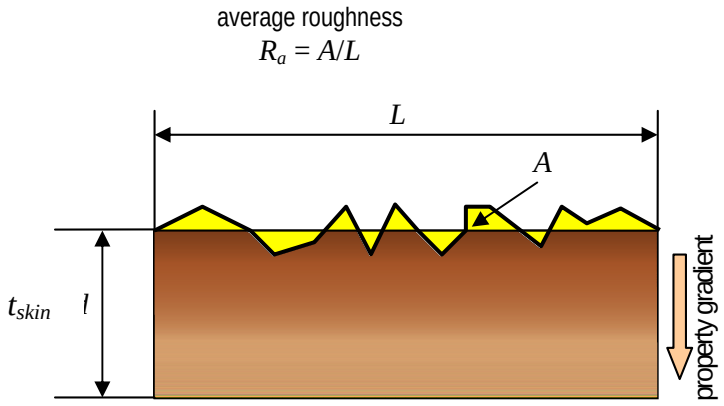

Fig. 32. Characterization of skin quality.

Regression analysis data for tensile and yield strength are presented in Table 11. With these equations the skin factor of any sample can be calculated from metallographic analysis only. Because only one as-cast surface was used in these experiments, the R^2 was very poor. Consequently these regression equations should only be considered an example.

Table 11. Regression Analysis for As-Cast Samples (Mold #2 Only)

Quantity	Intercept	t_{skin} (mm)	R_a	Std. error	Observations
UTS (ksi)	62.85	-7.19	0.14	2.36	15
YS (ksi)	45.45	-13.09	-0.008	3.21	15

CONCLUSIONS

The range of skin depth for the TWDI plates investigated is between 0.15 and 0.45mm. It was found that the skin depth decreases with increased test plate thickness.

The roughness increased with higher metallostatic pressure. Within the range of roughness investigated in this research (average *Ra* = 18.6μm) there was no clear trend on the tensile properties, other than the machined samples exhibiting higher properties than the as-cast ones.

The strength decreased with thicker casting skin and increased with thicker test plates. The tensile and yield strength skin factor was about 0.93. This should be viewed as an upper limit, as only one of the surfaces of the test plates was as-cast.

The results presented in this section are mostly semi quantitative because the “as-cast” test samples had in fact only one of four surfaces as-cast. A better test casting that will include more casting skin when tested “as-cast” should be designed.

MECHANISM OF CASTING SKIN FORMATION

As evident from the various microstructures presented in this report, the three main metallographic characteristics of the skin casting of ductile and compacted graphite iron are graphite degradation, graphite depletion and pearlitic rim. We believe that these microstructural changes can be explained by liquid state and solid state diffusion mechanisms.

During the residency of molten metal in the mold and before solidification begins oxygen or sulfur from the mold diffuses in the adjacent liquid shell of the casting and reacts with Mg, Ce or other graphite modifiers in the melt. This will induce graphite degradation in the following sequence: 1) SG degenerates to CG; 2) CG degenerates to lamellar graphite; 3) type A - lamellar graphite degenerates to type D.

Alternatively, the same diffusion processes can result in complete depletion of graphite in DI. This depletes the skin of ferrite nuclei during the solid state transformation and may result in a pearlitic rim.

Other elements (*e.g.* C or S) can diffuse in liquid or solid state producing carbon-rich layers in the casting. During the solid state transformation these layers become the pearlite rim.

The plausibility of this theory will be checked through calculations.

Graphite Degradation Rim

Let us start by examining some microstructures presented earlier in this report. From Fig.17 it is noted that as the metallostatic height increases from 0 to 1.5in., so does the skin thickness (red line on the figure). Let us first explore the graphite degradation rim. Graphite degeneration (degradation) can only occur because of:

- loss of Mg or Ce – possible causes are fading or chemical combination with S or O;
- poisoning by deleterious elements such as Te, Sb, As, etc.

In this case it is reasonable to assume that Mg from the melt was tied by oxygen or/and sulfur diffusing from the mold. A higher Mg level should result in thinner skin. Indeed, recent work[6] showed this to be true. Thus, the main cause of graphite degradation rim is Mg fading in the outer layer of the casting.

To verify this hypothesis a Mg diffusion model was developed. The basic assumptions of the model included: 1) Mg sink at mold/metal interface (there is enough oxygen; oxygen – Mg reaction is instantaneous); 2) No liquid convection; 3) Initial Mg residual of 0.019%. The diffusivity of Mg in liquid iron was taken as $2 \cdot 10^{-8}$ m^2/s. The local solidification time calculated with the Magmasoft code for the test sample in Fig. 7 was 70s.

The governing equation is the solute diffusion equation:

$$D\frac{\partial^2 C}{\partial x^2} = \frac{\partial C}{\partial t} \qquad \text{Equation 3}$$

where D is Mg diffusivity, C is composition, x is distance and t is time.

The results of the calculation are presented in Fig. 33a. Assuming the lower level of Mg required for CG formation to be 0.016%, the model predicts the thickness of the graphite degradation layer to be 2.3mm. The average measured graphite degradation rim is in the range of 0.7 to 2.6mm (see Fig. 20). Thus, diffusion calculations confirm the diffusion theory of the graphite degradation skin.

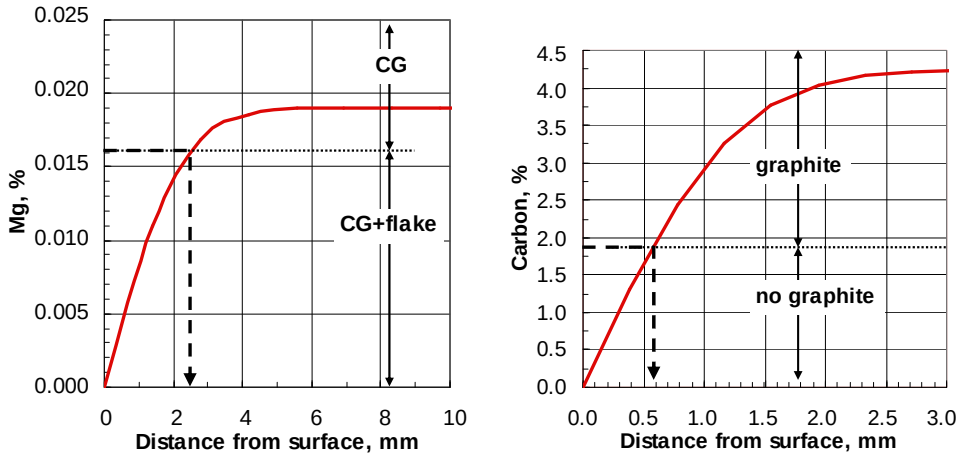

a) magnesium profile ***b) carbon profile***

Fig. 33. Magnesium and carbon content profile across the CGI test sample in Fig. 16.

It remains to explain the change in the thickness of the graphite degradation zone as a function of the metallostatic height (the edge effect for graphite degeneration) seen in Fig. 17. We propose that liquid convection in the solidifying metal determines the outcome, as follows. If high liquid convection occurs prior and during solidification, liquid rich in Mg is transported from the bulk into the surface layers of the casting and graphite degradation is minimal. However, if convection is low, liquid poor in Mg solidifies resulting in high graphite degradation. Indeed, for the particular casting configuration used in this research Magmasoft calculations suggest lower convection levels in the lower regions of the test sample because of the corner effects (Fig. 34).

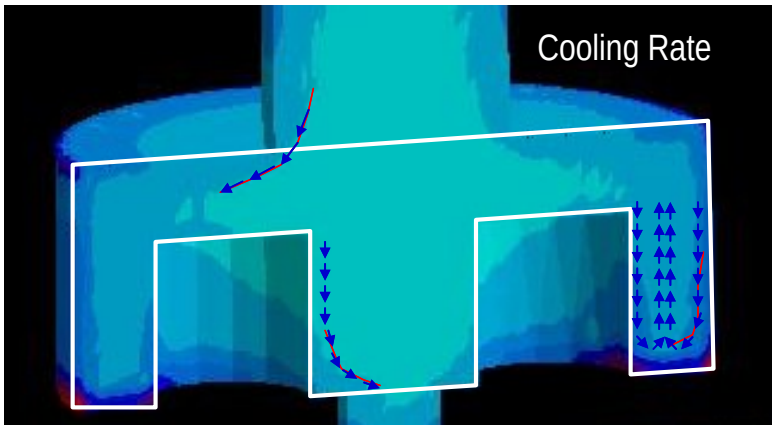

Fig. 34. Magmasoft calculated cooling rate and flow in the CGI test casting.

Graphite Depletion Rim

The cause for the graphite depletion rim must be carbon loss in the surface layer of the casting. Carbon loss is to be expected if there is an oxidizing atmosphere in the mold. This was indeed the case for resin bonded molds without carbonaceous additions used in this research. A carbon diffusion model similar to the one for magnesium discussed earlier was developed. The basic assumptions of the model included: 1) carbon sink at mold/metal interface (there is enough oxygen; oxygen – carbon reaction is instantaneous); 2) no liquid convection; 3) initial carbon content of 4.23%. The diffusivity of carbon in liquid iron was taken as $2 \cdot 10^{-8}$ m^2/s. The local solidification time calculated with the Magmasoft code for a DI plate having dimensions of 100x20x6mm was 18s.

The maximum solubility of carbon in austenite is 2.1%C for the Fe-C system at the eutectic temperature. Silicon decreases carbon solubility according to the relationship:

$$\Delta C_E^{Si} = -0.11 \cdot \%Si \qquad \text{Equation 4}$$

where ΔC_E^{Si} is the change in carbon solubility at point E (max. solubility of C in austenite) on the FeC diagram[13]. For 2.73%Si we calculate ΔC_E^{Si} = 0.3%, which gives a maximum solubility of 2.1 - 0.3 = 1.8%C. This is the minimum carbon content for graphite formation.

The results of the calculation are presented in Fig. 33b. It is seen that the carbon content decreases below 1.8%, which is the maximum limit for graphite formation, at a distance of 0.6mm from the surface. Thus, the predicted carbon depletion layer is 0.6mm thick. The average measured graphite depletion rim for thin DI reported earlier in this paper is in the range of 0.15 to 0.45mm (see Fig. 20). Thus, carbon diffusion calculations seem to confirm the diffusion theory of the graphite depletion skin.

Pearlitic Rim

Let us now turn to the pearlite rim. Two different mechanisms can be responsible for its formation:

1. carbon oxidation in the surface layer of the casting because of reaction with the mold atmosphere resulting in carbon depletion decreases the number of nuclei available for ferrite growth during the A1 transformation, and thus favors pearlite formation.

2. carbon or sulfur diffusion from the mold into the surface layer of the casting favors pearlitic transformation in the skin during cooling through the A1 temperature;

The first mechanism has been confirmed in the previous section. A simple diffusion calculation can be performed to check the second mechanism. Assuming the solid diffusivity of C in austenite of the order of $1.5 \cdot 10^{-10}$ m^2/s, and taking a local transformation time of 500s, the diffusion distance is calculated to be:

$$L = \sqrt{D \cdot t} = 0.3mm \qquad \text{Equation 5}$$

The average measured pearlitic rim is about 0.25mm (see Fig. 11).

Whether the carbon film on the surface of the advancing front of liquid cast iron reported in recent work[14] has any correlation to the casting skin is still to be explored.

ACKNOWLEDGMENTS

This work was made possible by a grant from the American Foundry Association. The authors are indebted to the members of the 5I Committee and of the Steering Committee (Ron Walling chair) for their support and many useful suggestions and comments. Stephanie Wills is grateful to Ashland Casting Solutions for the financial support during her Master of Sciences studies at OSU, and all authors are thankful for permission to use the Ashland casting laboratory. At the time the research was performed Dr. Juan Massone, permanently with the Univ. of Mar del Plata, Argentina, was a Fulbright Scholar at OSU.

REFERENCES

1. G.M. Goodrich and R.W. Lobenhofer, *Trans. AFS*, 110 (2002) pp 1003-1032
2. F. Mampaey, P. Li and E. Wittink, *Trans. AFS*, 111 (2003) paper 03-056
3. J.W. Torrance and D.M. Stefanescu, *Trans. AFS*, 112 (2004)
4. L.P. Dix, R. Ruxanda, J. Torrance, M. Fukumoto and D.M. Stefanescu, *Trans. AFS*, 111 (2003) pp 1149-1164
5. C. Labreque, M. Gagne, Javaid A. and Sahoo M., *Int. J. Cast Metals Res*. 16 (2003) 313
6. R.C. Aufderheide, R.E. Showman and M.A. Hysell, *Trans. AFS*, 113 (2005)
7. Flávia C. Duncan and J. Kroker, "Difficulties in Controlling and Measuring Flake Skin in CGI" WFO Technical Forum, Düsseldorf, Germany (2007)
8. Azterlan, Euskadia, Spain, Private Communication
9. C. Labrecque, M. Gagné, P.-M. Cabanne, C. François, C. Becret, and F. Hoffmann, *Int. J. of Metal Casting* 2 Issue 2 (2008)
10. D.M. Stefanescu and F.R. Juretzko, *Trans. AFS*, 115 (2007) paper 07-118
11. R.E. Ruxanda, D.M. Stefanescu, T.S. Piwonka, *Trans. AFS* 110 (2002) 1131
12. D.M. Stefanescu, Stephanie Collins and J. Massone, “Study of the Effect of the Casting Skin on the Tensile Properties of Light Weight Ductile Iron Castings” AFS Report (Jan. 2008)
13. 13.D.M. Stefanescu, “Thermodynamic Properties of iron-base Alloys”, ASM Handbook vol. 15, Casting (1988) 61-70
14. A. Habibollahzadeh and J. Campbell: *Trans. AFS*, 111 (2003) paper 03-021